RESEARCH ARTICLE

Prediction model of surface roughness of selective laser melting formed parts based on back propagation neural network

Wang Zhang[1] | **Chunwang Luo**[2] | **Qingyuan Ma**[3] | **Zhenqiang Lin**[1] | **Lan Yang**[3] | **Jun Zheng**[1] | **Xiaohong Ge**[1] | **Wei Zhang**[3] | **Yuangang Liu**[4] | **Jumei Tian**[5]

[1]College of Materials Science and Engineering, Xiamen University of Technology, Xiamen, China

[2]College of Electrical Engineering and Automation, Xiamen University of Technology, Xiamen, China

[3]State Key Laboratory of Powder Metallurgy, Central South University, Changsha, China

[4]College of Chemical Engineering, Huaqiao University, Xiamen, China

[5]Xiamen Medical College, Engineering Research Center of Fujian University for Stomatological Biomaterials, Xiamen, China

Correspondence
Jun Zheng and Xiaohong Ge, College of Materials Science and Engineering, Xiamen University of Technology, Xiamen, China.
Email: jason@3dmetalwerks.com and xhge@xmut.edu.cn

Wei Zhang, State Key Laboratory of Powder Metallurgy, Central South University, Changsha, China.
Email: waycsu@csu.edu.cn

Yuangang Liu, College of Chemical Engineering, Huaqiao University, Xiamen, China.
Email: ygliu@hqu.edu.cn

Jumei Tian, Engineering Research Center of Fujian University for Stomatological Biomaterials, Xiamen Medical College, Xiamen, China.
Email: tjm@xmmc.edu.cn

Abstract

In this article, selective laser melting (SLM) equipment is used to print 316L stainless steel parts under different process parameters, and the surface roughness of the parts is measured. Based on back propagation neural networks (BP neural networks, BPNN), the upper surface roughness prediction model is established. The laser power, scanning speed, and scanning interval are used as model input, and the surface roughness of the workpiece is output. This model can easily and quickly predict the surface roughness of SLM metal printing, with high prediction accuracy, and can provide a basis for the optimization of SLM process parameters.

KEYWORDS
BP neural network, prediction, SLM, surface roughness

JEL CLASSIFICATION
Materials science

1 | INTRODUCTION

SLM technology is a metal additive manufacturing technology that was patented by Dr. Konrad Wissenbach and Dr. Wilhelm Meiners of Germany. The metal parts are made by melting the micron-sized metal powder with high-energy laser beams and forming them according to the principle of stratification and superposition. Due to the mechanism of rapid solidification of powder, the grains in the shaped body are fine and the strength is higher than that of the casting.[1,2] SLM molded parts have high strength, precision, and good mechanical properties.[3] Compared with the limitations of materials used in other additive manufacturing technologies, laser-selective melting forming materials include not only a single metal powder, but also alloys, composite materials, and ceramics. Therefore, it is widely used in medical and health, aerospace, automobile manufacturing, mold manufacturing, and other fields.[4,5]

The surface roughness of SLM printed molded parts is an important indicator to measure the forming quality. Better surface quality can effectively reduce the cumulative effect of forming parts and increase the density of forming parts. Poor surface quality will influence the fluctuation of cladding layer surfacing, form larger pores, reduces the strength of the formed parts and mechanical properties, and restricts the development of the SLM technique.[6] To improve the surface morphology of SLM- forming parts, many scholars have studied the surface morphology of SLM-forming parts. Kruth[7,8] obtained high-quality surface morphology by laser remelting the surface of the print. Dadbakhsh[9] and other studies found that the surface of the gold test piece was affected by parameters such as laser power and scanning speed. In general, many factors the surface roughness of SLM-forming parts. The main factors are laser power, scanning speed, scanning distance, and powder layer thickness. Whip[10] surface roughness of components built with different profile processing parameters was characterized using non-destructive and destructive measurement techniques. Deng[11] used response surface methodology to study the effect of different machining parameters (laser power, scan speed, and incubation space) on the density and surface roughness of SLM-fabricated 316L stainless steel parts. Simoni[12] analyzed the effect of laser remelting on the surface roughness of parts while changing machine parameters such as laser power and scan settings, and found that laser remelting with optimized parameter settings can significantly improve the surface quality of SLM parts. These approaches have facilitated the development of SLM processes, but there is still room for improvement in smart optimization.

In the era of rapid development of science and technology, people's requirements for intelligence are getting higher and higher, and artificial intelligence has set off a new wave. Artificial neural networks (ANN) is a computational model that mimics biological neural networks. It evolved from the single-layer perceptron M-P model proposed in 1943 to a computing model that now has a multilayer perceptron network.[13–16] The computational power is greatly improved and can deal with complex nonlinear problems. It is widely used in model recognition, machine vision, speech recognition, and other artificial intelligence fields. A BP neural network is a feed-forward artificial neural network using an error back propagation algorithm, it has strong adaptive self-learning ability, superior fault tolerance, and robustness, and is the most widely used of the neural network models. BP neural networks structure is divided into three layers, namely, the input layer, hidden layer, and output layer, through the connection between each layer connection weights and threshold values, as shown in Figure 1. The basic principle is that the input vector flows through the hidden layer and the output layer of the inter-layer transfer function. If the demand is not met, the output value of the neuron is returned. The learning process is modified by modifying the connection weight and threshold value. The whole process continues until the output value meets the requirements and terminates. Gill[17] proposed a genetic algorithm technique based on ensemble back propagation to train artificial neural networks. Wang[18] established several different solar irradiance prediction model network structures based on BP neural networks. The most important thing is that the BP neural networks have a high self-learning and self-adaptive ability. Kim[19] established a BP neural network prediction model for predicting the height of robot welding bead, which shows that the neural network has a strong ability to find the laws existing in the sample, and its prediction ability is not inferior to the traditional statistical analysis method.
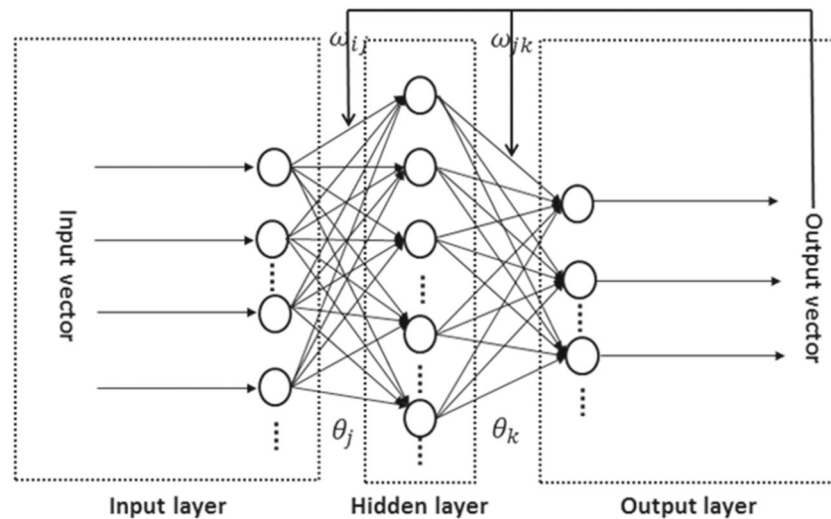
FIGURE 1   BP neural network structure

At present, the surface roughness of SLM-formed parts is basically measured directly by the roughness tester to obtain the surface roughness. This method of printing the formed parts first, and then obtaining the surface roughness, not only wastes materials, but also wastes staff operation and equipment working hours. In this study, the process parameters of SLM-formed parts are used as the input of the BP neural network, the surface roughness is the output, and a model for predicting the surface roughness of SLM-formed parts is constructed. Through the constructed prediction model, the surface roughness of the formed parts with different process parameters can be predicted without printing the formed parts. The method can not only regulate the process parameters and ensure the surface quality of the formed parts, but also save the cost, and contribute to promoting the development of laser selective melting and expanding the application scope of the neural network in the manufacturing industry.

2 | MEASUREMENT PRINCIPLE AND METHOD OF SURFACE ROUGHNESS OF FORMED PARTS

2.1 | Measurement principle

Surface roughness refers to the smaller spacing and peak-to-valley unevenness in the processed surface. The main parameters for measuring the surface roughness are: the arithmetic mean deviation of the profile (R_a), the maximum height of the profile (R_y), the 10-point height of the micro unevenness (R_Z) and so forth.

In the plane Cartesian coordinate system, a two-dimensional model of the surface contour of a part is established. A central line "m" is drawn on a certain length (L) so that the contour areas of the first and fourth quadrants are equal, rather than the middle line of a certain length L, as shown in Figure 2.

R_a refers to the abscissa of the length L selected on the surface profile, and the arithmetic means obtained by selecting the sum of the absolute values of n points within the sampling length. Theoretically, the larger n is, the more reliable the deviation of the arithmetic mean is obtained. R_z refers to the sum of the average of five adjacent peaks and five adjacent valleys on the part surface profile. R_y refers to the difference between the highest peak and the lowest valley depth in the selected area. In this study, according to the existing experimental equipment conditions, the maximum height R_y of the contour is selected as the parameter to study the surface roughness.

2.2 | Experimental equipment and materials

The experimental laser melting selection equipment adopts the WXL-120 equipment independently developed by Xiamen Wuxinglong Technology Co., Ltd., as shown in Figure 3. The processing size of the equipment is
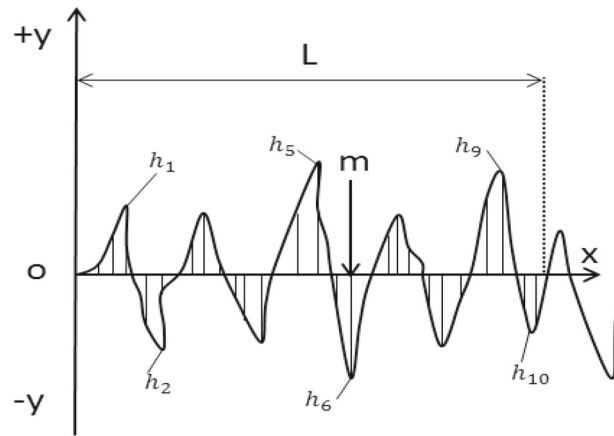
FIGURE 2   Part surface contour

FIGURE 3   WXL-120 equipment

120 mm × 120 mm × 100 mm, which is mainly composed of an optical path system, laser scanning system, gas protection system, powder spreading system, forming cylinder, powder feeding cylinder, powder recovery bar, motion mechanism, and upper computer control system. Users can independently adjust equipment parameters and flexibly choose metal materials. In this experiment, 316L stainless steel spherical powder prepared by AVIC Metal Powder Metallurgy Technology (Beijing) Co., Ltd. was used as the printing material. The standard grade of 316L is 022Cr17Ni12Mo2, which mainly contains Cr, Ni, and Mo, and has excellent corrosion resistance, especially pitting resistance-, and excellent work hardening performance. The particle size range is 15–53 μm, and the median diameter (D50) is 34.57 μm. Figure 4 is the shape of the 316L alloy powder. The powder is uniform and high in sphericity. It has good fluidity and is good for forming. Figure 5 is a particle size distribution curve.

In order to ensure the fluidity of the powder during the printing process, the powder was placed in a vacuum drying oven at high temperature for heating and holding for a period of time before the experiment to achieve the effect of drying. After the powder is dried, put it in the printing equipment to print. According to the previous basic experiments and the characteristics of WXL-120 equipment, combined with the research content of this article, using 80–110 W laser, 600–1200 mm/s scanning speed, 0.03–0.07 mm scanning spacing, printing 48 different process parameters of 10 mm × 10 mm × 10 mm experimental piece. The selection of specific parameters is shown in Table 1.
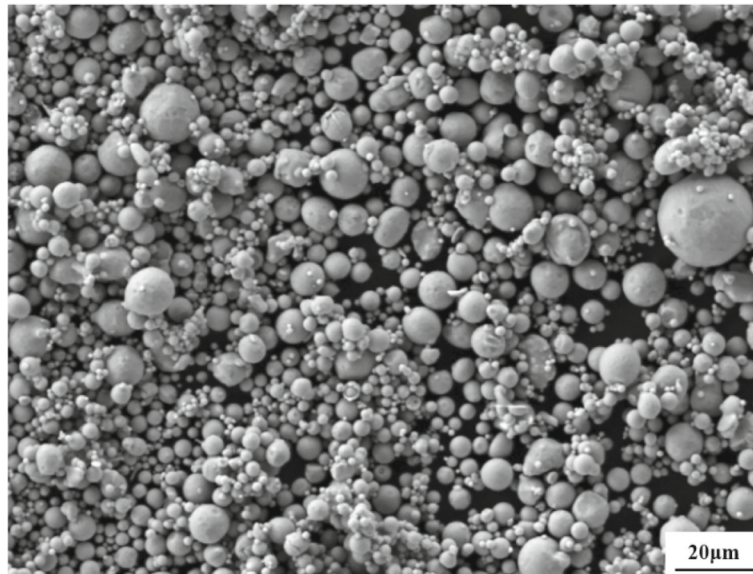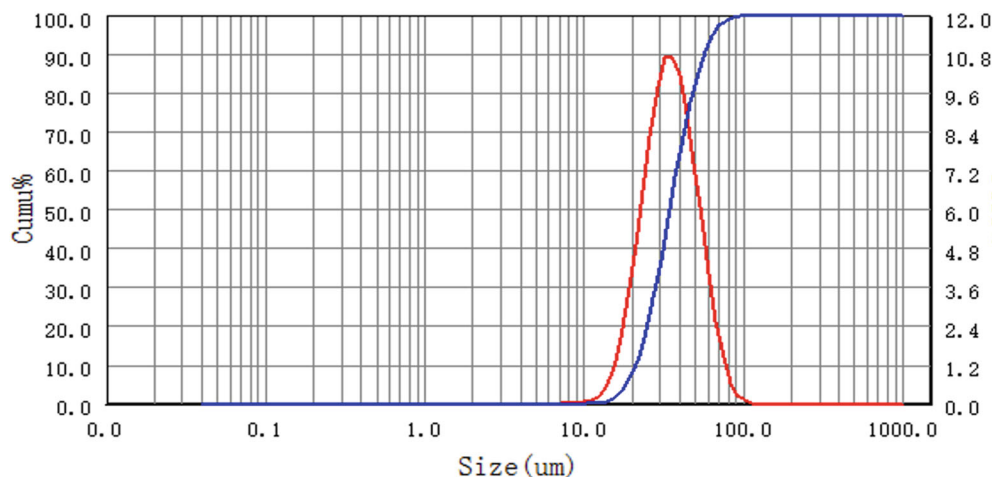

FIGURE 4   316L powder form

FIGURE 5   Particle size distribution curve

TABLE 1 Process parameters value range

Laser power (W)	Scanning speed (mm/s)	Scanning pitch (mm)
80, 90, 100, 110	600, 800, 1000, 1200	0.03, 0.05, 0.07

Nitrogen is used as a protective gas during the printing process, and the oxygen content is controlled below 0.24%. The scanning strategy adopts interlaced scanning, and the powder layer thickness is set to 30 μm. After printing, it will be shown in Figure 6.

FEI Quanta FEG 250 scanning electron microscope (SEM) was used to investigate the SLM-formed samples' surface topography. The 2D/3D surface topographies of the upper surfaces were examined by a NanoMap-1000 WLI profilometer to evaluate the surface quality, its measurement settings are shown in Table 2.

2.3 | Experimental method

There are many measurement methods of surface roughness, such as contact measurement and noncontact measurement, and observation and comparison methods.[20] Combined with the existing equipment resources for the experiment and the characteristics of the materials to be measured, this article adopts the contact measurement method. The contact measurement is generally based on the stylus measurement method. The stylus can be used to obtain the required information and calculate the roughness value. In this experiment, the Ji-Tai 0918 roughness tester was used to measure the roughness of the parts, as shown in Figure 7. The surface roughness meter can directly measure the height from the peak to the valley bottom of the surface, the required measurement area is small, the range is $0 \sim 6500$ μm, and the accuracy is 0.2 μm.

In the experiment, a total of five areas from four peripheries and the center of the upper surface of the formed part are selected, as shown in Figure 8. Use a surface roughness tester to measure the R_y value of the selected

FIGURE 6 Test pieces

TABLE 2 Measurement settings for the NanoMap-1000 WLI profilometer

Measured area		5 mm*5 mm
Scanning pitch		10 μm
Stepping pitch		16.7 μm
Objective	Magnification	0

F I G U R E 7   Surface roughness tester
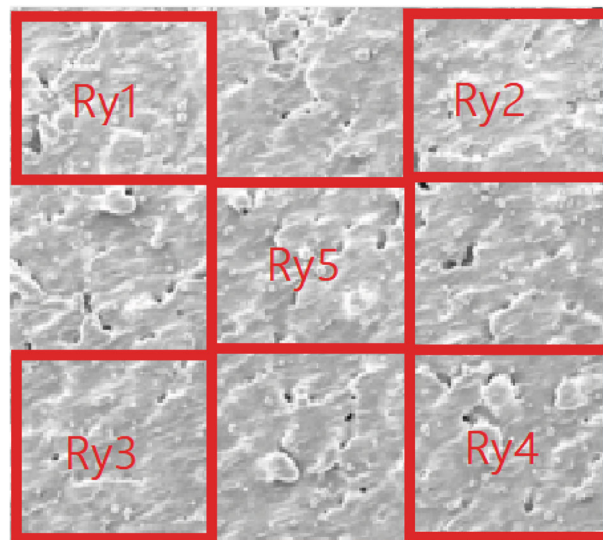
F I G U R E 8   Part surface measurement area

area and take the average, as shown in Equation (1), which is the value of the upper surface roughness of each formed part.

$$R_{\mathrm{y}} = \frac{R_{y1} + R_{y2} + R_{y3} + R_{y4} + R_{y5}}{5}. \tag{1}$$

3 | BP NEURAL NETWORK MODEL ESTABLISHMENT AND RESULT ANALYSIS

3.1 | Selection of input

There are more than 100 factors that affect the quality of laser selective melting molding, but in fact, there are only a dozen factors that affect the molding effect.[21] The energy density (E) is the most direct factor affecting the quality of

laser-selected and melted parts. It can be seen from Equation (2) that the energy density is determined by the laser power (P), the scanning speed (V), and the scanning distance (H).

$$E = \frac{4P}{\pi VH}. \tag{2}$$

Laser power (P) is the premise of laser selective melting printing, and sufficient laser power is a necessary condition for metal powder melting. When the laser power is low, the powder obtains less energy, and the powder obtained in the molten pool cannot be completely melted, resulting in a spheroidization effect. Excessive laser power will cause excessive sintering of the printed parts. Therefore, selecting the laser power within a reasonable range can ensure that the powder is fully melted without causing over-burning, to complete high-quality printing.

The scan speed (V) is the speed at which the laser moves and it determines the time it takes for the laser to melt the powder. The low scanning speed will lead to the metal powder obtaining a high enough energy density, which will cause the local liquid vaporization of the molten pool, the bubbles will not be discharged in time, and the metallurgical pores will be formed inside the part. The high scanning speed makes the residence time in the molten pool too short, and the metal liquid solidifies without being fully wetted, resulting in a keyhole. A suitable scan speed can obtain a good metallurgical combination to meet the needs of printing quality.

The scanning spacing (H) is the distance of the light spot when the laser scans adjacent cladding tracks, which determines the overlap between adjacent cladding tracks. The scanning speed spacing is too small and the overlap is too frequent, which not only makes the energy density of the cladding track too large, but also affects the efficiency of the line. The scanning distance is too large, the overlap is too sparse, and there are pores or even incomplete overlap at the overlap of the cladding track, which reduces the surface quality. Appropriate scanning spacing can fully overlap adjacent cladding tracks, smooth the surface, and improve printing quality.

In a certain range, if the energy density is too low, the powder cannot melt completely, and the surface tension of the liquid is greater than the diffusion stress, spheroidization will occur. The spheroidization effect will affect the quality of the next powder spreading. The powder is not spread sufficiently and many pores are formed. The appearance of the cumulative effect will deteriorate the surface morphology of the formed part, resulting in poor surface quality. As shown in Figure 9A, the printed part with 110 W laser power, 600 mm/s scanning speed, and 0.03 mm scanning pitch, the value of the average surface roughness (S_a) is 53.258 μm. Sufficient energy density can spread the components of the molten pool and eliminate spheroidization. The upper and lower layers can be ideally connected to reduce the effect of cumulative effects and improve the surface quality of the formed parts. As shown in Figure 9B, the printed with 80 W laser power, 1200 mm/s scan speed, and 0.07 mm scan pitch, the sample printed with sufficient energy density has a smooth surface and clear melting channels, and the S_a value of the sample is 37.819 μm. It can be seen from the 2D/3D topographies of the samples' surfaces that the surface quality can be significantly improved by adjusting the process parameters.

It can be seen that the energy density is closely related to the quality of the SLM molded part, therefore, the laser power, scanning speed, and scanning interval can be set as the input items of the surface roughness prediction model.

3.2 | BP neural network construction

The effects of laser power, scanning speed, and scanning distance on the surface roughness of SLM forming parts were analyzed. The three variables of laser power, scanning speed, and scanning distance were taken as the input parameters, and the surface roughness was taken as the output. A BP neural network model with three inputs and one output was established. There are many transfer functions of the BP neural network, the input value of the log-sigmoid function can take any value, and the output value is between 0–1. The input value of the tan-sigmod type transfer function tansig can take any value, and the output value is between −1 and 1. When the transfer function uses the tansig function, the error is smaller than that of the log-sigmoid function, and the output value range is larger. Therefore, in the training, the hidden layer transfer function uses the tansig function, and the neurons in the output layer use the purelin function. Its input can take any value, and the entire output of the network can take any value. The determination of hidden layer nodes is the key to success or failure. If the number is too small, the information obtained by the network to solve the problem is too small, and the number is too large, which not only increases the training time, but also may cause the problem of transition matching, that is, the test error large, and the generalization ability decreases. The general principle is that on the basis of correctly reflecting the input–output relationship, a smaller number of hidden layer nodes should be selected
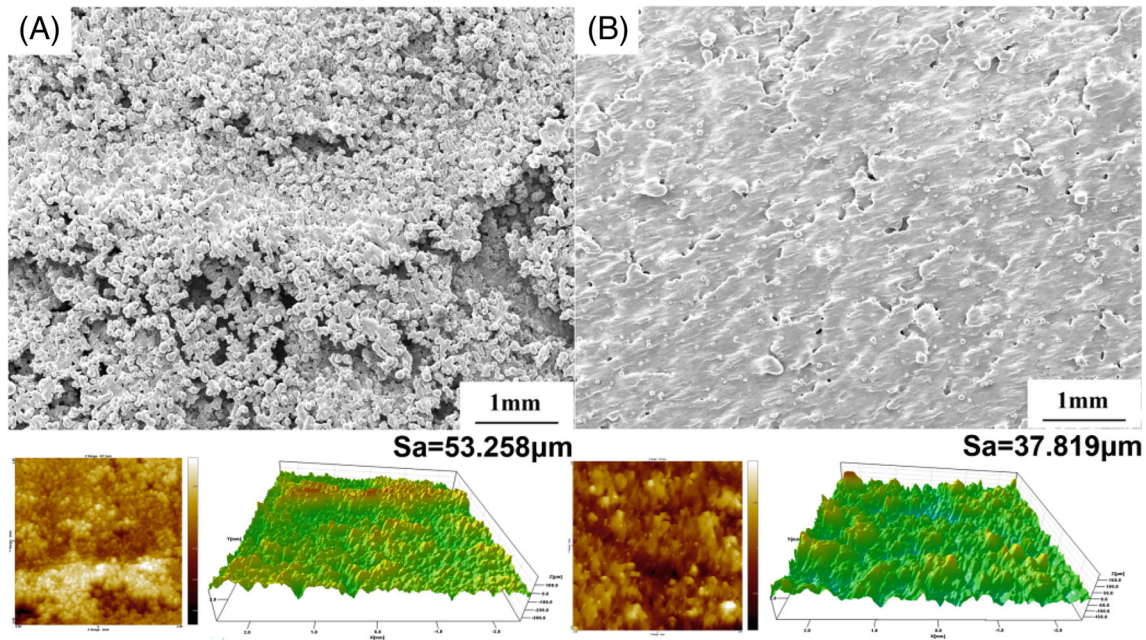
FIGURE 9 Macroscopic appearances and 2D/3D topographies of samples' surfaces

to make the network structure simple. In this article, a small number of nodes is set first, the network is trained, and the nodes are added after repeated attempts until the learning error is no longer significantly reduced. Finally, the hidden layer of the network is set to a single layer of 9 nodes. The network structure is shown in Figure 10.

3.3 | Model prediction results and analysis

Based on the measured surface roughness data, 10 of the 48 samples were randomly selected and substituted into the model for verification to verify the reliability of the predicted results of the surface roughness of the samples.

After importing the data, train the BP neural network model and provide 10 sets of verification data input samples to the BP network to obtain the predicted value of the surface roughness, as shown in Table 3.

The network prediction curve is shown in Figure 11. The graph can be seen intuitively to see that the expected surface roughness and the predicted value curve have a high degree of fitting. At the same time, take the parameters corresponding to the printed parts with the largest error, set the same printing parameters of the machine, and repeat the printing to measure the R_Z. The comparison found that the change of R_Z is small, indicating that the machine environment has no major impact on the printed parts. In order to verify the reliability and generalization of the model, the external data is verified. Keep two of the three input items unchanged, change one of the input items, and in turn, do six sets of parameter experiments, the specific parameters are shown in Table 4, and input samples into the BP neural network to obtain the
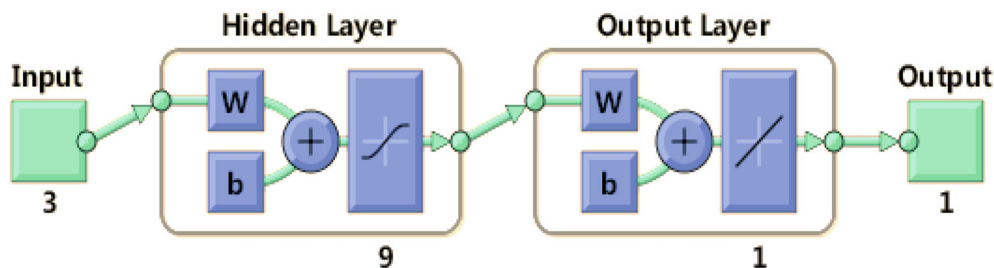

FIGURE 10 Neural network

TABLE 3 Network prediction results and errors

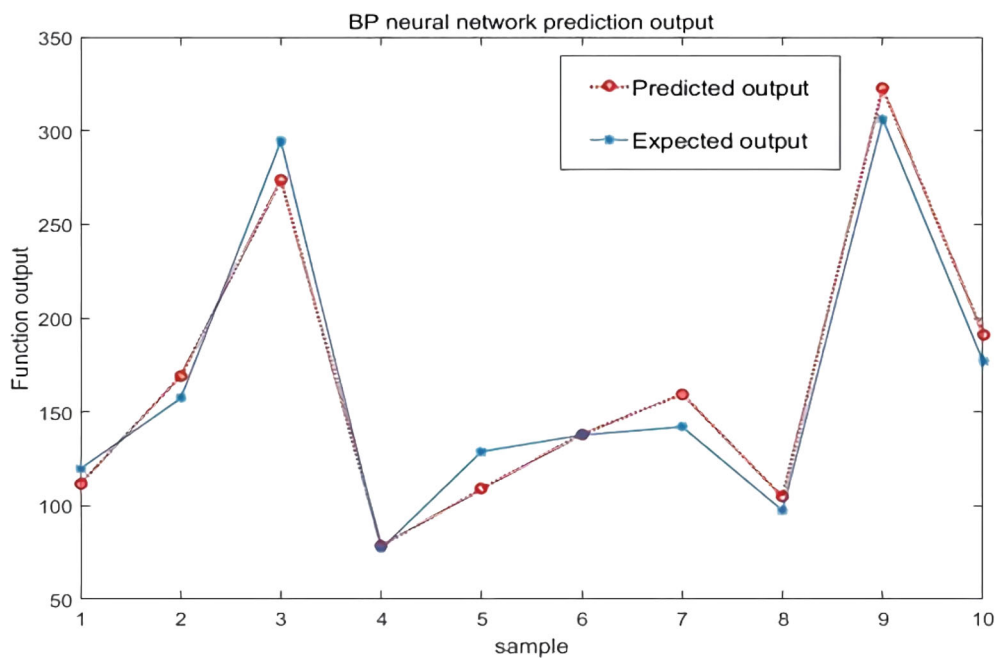| Numbering	Prediction (μm)	Expectations (μm)	Absolute error (μm)	Relative error (%)
1	111.7	119.6	7.9	6.6
2	169	157.2	11.8	7.5
3	273.8	294.4	20.6	6.99
4	78.51	77	1.51	1.96
5	108.8	128.8	20	15.52
6	138.1	137.6	0.5	0.36
7	159.4	142	17.4	12.25
8	104.6	97.4	7.2	7.39
9	322.7	306.2	16.5	5.39
10	191.3	177	14.3	8.08

FIGURE 11 Network prediction curve

predicted value of surface roughness. Comparing the measured sample surface roughness data, the absolute error and relative error are calculated, as shown in Table 5. The relative errors are basically less than 10%, indicating that the model has high prediction accuracy and reliable prediction results.

3.4 | Study on the relationship between surface roughness and relative density

In the experiment, the relative density of 48 small squares was measured by the drainage method. First, the wet weight m_1 of the printed piece in distilled water and the weight m_0 after drying were measured. The value measured by the electronic balance model BSM220.4 can be accurate to 0.1 mg, as shown in Figure 12.

According to Archimedes' principle, the relative density ρ of the molded part is calculated, as shown in Equation (3), ρ_1 is the standard atmospheric pressure distilled water density of 1 g/cm^3, ρ_0 is the standard density of 316L stainless steel, and the experiment takes 7.98 g/cm^3.

TABLE 4 Modified parameters

Numbering	Laser power (W)	Scanning speed (mm/s)	Scanning pitch (mm)
1	120	1000	0.05
2	70	1000	0.05
3	100	700	0.05
4	100	1300	0.05
5	100	1000	0.04
6	100	1000	0.06

TABLE 5 Network prediction results and errors

Numbering	Prediction (μm)	Expectations (μm)	Absolute error (μm)	Relative error (%)
1	133.5	124.3	9.2	7.4
2	211.9	237.6	25.7	10.8
3	175.3	192.7	17.4	9.0
4	214.1	203.5	9.6	4.7
5	331.5	311.8	19.7	6.3
6	291.7	268.2	23.5	8.7

FIGURE 12 BSM220.4 electronic balance

$$\rho = \frac{m_0 \rho_1}{(m_0 - m_1)\rho_0} \times 100\%. \tag{3}$$

The relative density and roughness of 48 groups of blocks were calculated and measured as shown in Table 6 below. When the relative density reaches the maximum of 96.811%, the surface roughness under the corresponding parameters is 219.3 μm, which is not the minimum. When the surface roughness reaches a minimum of 77, the relative density under the corresponding parameters is 82.496%, which is not the maximum. Comprehensive data analysis shows that there is no direct relationship between relative density and surface roughness.

T A B L E 6 Values for surface roughness and relative density

Numbering	Laser power (W)	Scanning speed (mm/s)	Scanning pitch (mm)	Surface roughness (μm)	Relative density (%)
1	80	600	0.03	226.8	69.679
2	80	800	0.03	191.3	75.317
3	80	1000	0.03	172.5	79.328
4	80	1200	0.03	149.8	82.974
5	80	600	0.05	203.3	68.934
6	80	800	0.05	176.1	70.481
7	80	1000	0.05	142.8	73.436
8	80	1200	0.05	119.6	76.153
9	80	600	0.07	181.4	66.719
10	80	800	0.07	153.6	69.373
11	80	1000	0.07	134.9	71.543
12	80	1200	0.07	121.2	74.221
13	90	600	0.03	194.7	75.696
14	90	800	0.03	177.2	79.154
15	90	1000	0.03	153.8	82.536
16	90	1200	0.03	140.6	86.324
17	90	600	0.05	157.2	70.259
18	90	800	0.05	135.8	73.213
19	90	1000	0.05	113.3	76.256
20	90	1200	0.05	96.2	80.272
21	90	600	0.07	123.2	69.246
22	90	800	0.07	107.5	71.324
23	90	1000	0.07	91.8	74.913
24	90	1200	0.07	77	82.496
25	100	600	0.03	317.1	79.247
26	100	800	0.03	294.4	82.056
27	100	1000	0.03	234.3	84.217
28	100	1200	0.03	187.2	89.742
29	100	600	0.05	216.9	77.034
30	100	800	0.05	181.3	80.722
31	100	1000	0.05	156.9	81.568
32	100	1200	0.05	148	83.015
33	100	600	0.07	146.4	74.756
34	100	800	0.07	132.7	76.003
35	100	1000	0.07	119.2	78.884
36	100	1200	0.07	128.8	80.035
37	110	600	0.03	337.4	91.654
38	110	800	0.03	219.3	96.891
39	110	1000	0.03	135.5	88.064
40	110	1200	0.03	179.1	85.226
41	110	600	0.05	306.2	88.354
42	110	800	0.05	177	93.983
43	110	1000	0.05	97.4	87.335
44	110	1200	0.05	142	84.984
45	110	600	0.07	251.3	88.378
46	110	800	0.07	137.6	91.554
47	110	1000	0.07	88.4	84.973
48	110	1200	0.07	126.3	81.549

4 | CONCLUSION

In this article, based on the diagnosis idea of the neural network, the surface roughness prediction model of SLM printed parts was established with laser power, scan speed, and scan spacing as input and surface roughness as output. The surface roughness is measured and calculated by sandblasting roughness meter. By comparing the predicted roughness values of neural network samples, the average error is calculated to be 7.20%. Meanwhile, the external data of the model are verified, and the predicted error of the model is calculated to be within 11%, which verifies the accuracy, feasibility, and generalization of the prediction model. It is verified that there is no direct relationship between surface roughness and relative density in this group of test pieces. The prediction model established in this article can predict the surface roughness of SLM forming parts with different process parameters without printing the forming parts. This method can not only control the process parameters, and ensure the surface quality of the molded parts, but also save the cost, and provide technical references for improving the surface quality of printed products. There are many factors affecting the surface roughness of SLM-forming parts. To improve the prediction model, it is necessary to introduce more factor variables (such as powder layer thickness) as input to expand the prediction range of the model, and improving the prediction accuracy of model surface roughness is a new challenge.

AUTHOR CONTRIBUTIONS
Wang Zhang: Conceptualization (equal); data curation (equal); methodology (equal); validation (equal); writing – original draft (equal); writing – review and editing (equal). **Chunwang Luo:** Data curation (equal); methodology (equal); validation (equal). **Qingyuan Ma:** Data curation (equal); supervision (equal). **Zhenqiang Lin:** Formal analysis (equal); validation (equal). **Lan Yang:** Investigation (equal); supervision (equal). **Jun Zheng:** Conceptualization (equal); project administration (equal); writing – review and editing (equal). **Xiaohong Ge:** Conceptualization (equal); supervision (equal). **Wei Zhang:** Conceptualization (equal); project administration (equal); validation (equal). **Yuangang Liu:** Project administration (equal); writing – review and editing (equal). **Jumei Tian:** Project administration (equal); validation (equal).

CONFLICT OF INTEREST
The authors declare no conflict of interest.

DATA AVAILABILITY STATEMENT
The data presented in this study are available upon request from the corresponding author.

ORCID
Wang Zhang https://orcid.org/0000-0002-6860-1692
Jun Zheng https://orcid.org/0000-0002-7352-955X

REFERENCES
1. Dai D, Dongdong G. Thermal behavior and densification mechanism during selective laser melting of copper matrix composites: simulation and experiments. *Mater Des.* 2014;55:482-491.
2. Vandenbroucke B, Kruth J-P. Selective laser melting of biocompatible metals for rapid manufacturing of medical parts. *Rapid Prototyp J.* 2007;13(4):196-203.

WILEY Engineering Reports Open Access

3. Sun TT, Yang YQ, Su XB, et al. Research of densification of 316L stainless steel powder in selective laser melting process. *Laser Technol*. 2010;34(4):443-446. (in Chinese).

4. Ren X-W, Zeng L, Wei Z-M, Xin X-Z, Wei B. Effects of multiple firings on metal-ceramic bond strength of co-Cr alloy fabricated by selective laser melting. *J Prosthet Dent*. 2016;115(1):109-114.

5. Keun-Taek O, Kang D-K, Choi G-S, et al. Cytocompatibility and electrochemical properties of Ti–au alloys for biomedical applications. *J Biomed Mater Res*. 2007;83B(2):320-326.

6. Mumtaz K, Hopkinson N. Top surface and side roughness of Inconel 625 parts processed using selective laser melting. *Rapid Prototyp J*. 2009;15(2):96-103.

7. Yasa E, Kruth J-P, Deckers J. Manufacturing by combining selective laser melting and selective laser erosion/laser re-melting. *CIRP Ann*. 2011;60(1):263-266.

8. Kruth J, Yasa E, Deckers J. Roughness improvement in selective laser melting. Proceedings of the 3rd International Conference on Polymers and Moulds; 2008:170-183; Ku LeUven.

9. Dadbakhsh S, Hao L, Jerrard PGE, Zhang DZ. Experimental investigation on selective laser melting behavior and processing windows of in situ reacted Al/Fe$_2$O$_3$ powder mixture. *Powder Technol*. 2012;231:112-121.

10. Whip B, Sheridan L, Gockel J. The effect of primary processing parameters on surface roughness in laser powder bed additive manufacturing. *Int J Adv Manuf Technol*. 2019;103:4411-4422.

11. Deng Y, Mao Z, Yang N, Niu X, Lu X. Collaborative optimization of density and surface roughness of 316L stainless steel in selective laser melting. *Materials*. 2020;13:1601.

12. Simoni F, Huxol A, Villmer FJ. Improving surface quality in selective laser melting based tool making. *J Intell Manuf*. 2021;32:1927-1938.

13. McCulloch WS, Pitts W. A logical calculus of the ideas immanent in nervous activity. *Bull Math Biophys*. 1943;5:115-133.

14. Minsky M, Papert S. *Perceptron: An Introduction to Computational Geometry*. The MIT Press; 1969.

15. Werbos P. *Beyond Regression: New Tools for Prediction and Analysis in the Behavior Science*, Doctoral Dissertation. Harvard University; 1974.

16. Hinton GE, Salakhutdinov RR. Reducing the dimensionality of data with neural networks. *Science*. 2006;313(5786):504-507.

17. Gill EJ, Singh EB, Singh ES. Training back propagation neural networks with genetic algorithm for weather forecasting. Proceedings of the IEEE 8th International Symposium on Intelligent Systems and Informatics; 2010:465-469; IEEE.

18. Wang Z, Wang F, Su S. Solar irradiance short-term prediction model based on BP neural network. *Energy Procedia*. 2011;12:488-494.

19. Kim IS, Son JS, Park CE, Lee CW, Prasad YKDV. A study on prediction of bead height in robotic arc welding using a neural network. *J Mater Process Technol*. 2002;130:229-234.

20. Rehme O, Emmelmann C. Reproducibility for properties of selective laser melting products. Proceedings of the 3rd International WLT-Conference on Lasers in Manufacturing, Munich; 2005:1-6.

21. Aboulkhair NT, Everitt NM, Ashcroft I, Tuck C. Reducing porosity in AlSi10Mg parts processed by selective laser melting. *Addit Manuf*. 2014;1-4:1-4.